Steps For Civil, Constructions and Environmental Engineering (SCCEE)
ISSN: 3005-8198 (online) / 3005-818X (print)
Volume 2, Issue 1 (January – March 2024), pp: 1-11

Research Article

Hydrothermal Synthesis of Hedgehog-Shaped ZnS Nanostructures: Structural Characterization and Photocatalytic Applications in Environmental Engineering

Marzieh Haghverdi [a], Akram Karbalaee Hosseini [b*], Azadeh Tadjarodi [c]

Research Laboratory of Inorganic Materials synthesis, Department of Chemistry, Iran University of Science and Technology, Tehran, Iran.

E-mail: Marzieh haghverdi@yahoo.com [a], akram5206@yahoo.com [b*], tajarodi@iust.ac.ir [c]

Received: 16 November 2023 | Revised: 26 December 2023 | Accepted: 17 January 2024 | Published: 12 February 2024

Abstract

The development of efficient photocatalysts for wastewater treatment is a critical challenge in environmental engineering. In this study, hedgehog-shaped zinc sulfide (ZnS) nanostructures were synthesized via a hydrothermal method using zinc nitrate hexahydrate and thiosemicarbazide as precursors. The products were systematically characterized using a variety of analytical techniques, including FT-IR, XRD, SEM, TEM, and UV–Vis. XRD analysis confirmed the formation of phase-pure ZnS with a wurtzite structure, while SEM and TEM images revealed hierarchical microspheres decorated with radially oriented nanorods of approximately 5 nm diameter. Optical analysis revealed a significant blue shift at approximately 290 nanometers and an augmented band gap, suggesting the presence of pronounced quantum confinement effects. The photocatalytic activity of the ZnS nanostructures was evaluated through the degradation of methyl orange dye under UV irradiation, achieving ~75% removal within 5 hours. The hierarchical hedgehog-shaped morphology of the samples provided enhanced light scattering and a high density of active sites, which improved photocatalytic efficiency in comparison with conventional ZnS nanostructures. These findings underscore the potential of ZnS-based nanostructures as sustainable photocatalysts for environmental remediation. Their distinctive architecture renders them well-suited for applications in wastewater treatment, dye removal, and integration into solar-driven photocatalytic systems. This work underscores the significance of morphology-controlled semiconductor nanostructures in propelling green technologies for environmental engineering.

Keywords: *Zinc Sulfide (ZnS) Nanostructures; Hydrothermal Synthesis; Hedgehog Morphology; Photocatalysis; Wastewater Treatment.*

*** Correspondence Author**

Cite This Article: Haghverdi, M., Hosseini, A. K., & Tadjarodi, A. (2024). Hydrothermal Synthesis of Hedgehog-Shaped ZnS Nanostructures: Structural Characterization and Photocatalytic Applications in Environmental Engineering. *Steps For Civil, Constructions and Environmental Engineering*, *2*(1), 1-11. https://doi.org/10.61706/sccee12011207

Introduction

Zinc sulfide (ZnS) is a II–VI semiconductor with a bandgap energy of 3.7 electronvolts at 300 kelvin and notable performance as a phosphor host material (Ibupoto et al., 2013). The material's optical transparency in the visible range and its favorable luminescence properties render it highly suitable for optoelectronic and photonic applications. ZnS has been the subject of extensive research in the fields of photocatalysts, solar window layers, optical coatings, electroluminescent devices, and photoconductors (Abd Al-Zahra & Al-Sammarraie, 2021). Furthermore, ZnS doped with particular cations demonstrates triboluminescence, defined as the emission of bright light under mechanical stress, which suggests its application in stress sensing and smart material systems (C. Jiang et al., 2007).

The focus on nanostructured ZnS has increased in recent years due to the strong correlation between its physical and optical properties and the dimensions and morphology of its particles. Advancements in synthetic techniques, including ultrasonic, hydrothermal, sonochemical, and mechanochemical methods, have facilitated the precise control over ZnS in zero-, one-, and two-dimensional forms (H. Wang et al., 2009). One-dimensional nanostructures, including nanorods, nanowires, nanotubes, and nanoribbons, are of particular interest for photocatalytic applications due to their anisotropic growth, high surface-to-volume ratios, and enhanced electron transport pathways. ZnS nanocrystals (NCs) have been shown to efficiently generate electron–hole pairs upon light exposure, rendering them effective photocatalysts for environmental remediation. Their capacity to degrade halogenated benzene derivatives, p-nitrophenol, and dyes during wastewater treatment has been extensively documented (Boulkroune et al., 2019; Houshmand & Emrooz, 2019; Isac & Enesca, 2022; Kozhevnikova et al., 2022; Lee & Wu, 2017; Motejadded Emrooz & Rahmani, 2017; Riazian, 2023; Riazian & Yekrangisendi, 2023; Sabaghi et al., 2018; Ücker et al., 2023). Moreover, defect engineering, such as sulfur vacancies, has enabled visible-light-driven hydrogen production, thereby extending ZnS applications into the domain of clean energy (G. Wang et al., 2015).

ZnS nanoparticles have also been explored for their potential in rapid optical switches and nonlinear devices, a property attributable to their tunable refractive indices. However, the majority of reported ZnS nanoparticles rely on organic capping agents, which influence surface and optical properties. In the pursuit of tailoring optical emission and stabilizing unique crystalline phases, researchers have employed strategies such as rare-earth doping (Viswanath et al., 2014) and interface engineering (Liang et al., 2012).

Notwithstanding these advances, studies on complex three-dimensional morphologies remain limited. Specifically, hedgehog-shaped ZnS nanostructures—consisting of radially oriented nanorods assembled into microspheres—have been shown to offer an unusually high density of active sites and multidirectional light-scattering ability, which could enhance photocatalytic efficiency in comparison to conventional nanorods or nanowires.

In this study, we present the hydrothermal synthesis of hedgehog-shaped ZnS nanostructures and evaluate their photocatalytic activity through the degradation of methyl orange dye under UV irradiation. The objective of this study is to demonstrate how hierarchical ZnS morphologies influence band gap characteristics and photocatalytic efficiency, thereby contributing to the design of advanced nanostructures for water purification applications.

Materials and Methods

Materials

All chemical reagents utilized in this study were procured from Merck Co. and employed without further purification. Zinc nitrate hexahydrate was utilized as the zinc source, while thiosemicarbazide was employed as the sulfur source. The hydrothermal synthesis process utilized ethylene diamine and distilled water as solvents.

Synthesis of ZnS Nanostructures via Hydrothermal Method

The ZnS nanostructures were synthesized through a hydrothermal route. In a typical procedure, 2 mmol of zinc nitrate hexahydrate and 3 mmol of thiosemicarbazide were dissolved in a mixed solvent of ethylene diamine and distilled water, maintaining a volume ratio of 3:2. The homogeneous solution that resulted from this process was transferred into an 80-mL Teflon-lined stainless-steel autoclave. The autoclave was then sealed and placed in an oven set at 200°C for a period of 10 hours.

Subsequent to the hydrothermal reaction, the autoclave was cooled naturally to room temperature. The resulting precipitate was collected and washed repeatedly with absolute ethanol and distilled water to ensure the removal of any residual impurities. Subsequently, the washed product underwent a drying process under vacuum conditions at a temperature of 200°C, a step that resulted in the formation of the final ZnS nanostructures.

Photocatalytic Activity Evaluation

The photocatalytic performance of the synthesized ZnS nanostructures was assessed through the degradation of methyl orange dye under UV irradiation. The elimination of nitrogen-containing dyes from

aqueous environments is of particular significance, as these dyes have the potential to generate toxic and carcinogenic compounds.

A methyl orange stock solution with a concentration of 3.75 parts per million (ppm) was prepared by first dissolving 0.00375 g of the dye in 1,000 mL of distilled water. For each photocatalytic test, 0.07 g of the synthesized ZnS nanostructures was added to 100 mL of the dye solution. Subsequently, the suspension was exposed to UV irradiation, with a power of 160 W, for varying time intervals to monitor the degradation process.

Characterization Techniques

The structural, morphological, and optical properties of the synthesized ZnS nanostructures were investigated using the following techniques (**Figure 1**):

- X-ray Diffraction (XRD): Phase identification was performed using a Jeol JDX-8030 diffractometer equipped with graphite-monochromatized Cu Kα radiation (λ = 1.541874 Å).
- The following is a synopsis of the Transmission Electron Microscopy (TEM) methodology. Transmission electron microscopy (TEM) images were obtained using a Philips CM 120 Eb Leo-912 microscope operated at an accelerating voltage of 120 kilovolts (H. Wang et al., 2009).
- UV–Visible Spectroscopy (UV–Vis): Absorption spectra were recorded with a Shimadzu UV–2550-8030 spectrophotometer, using a slit width of 5.0 nm and a light source wavelength of 360.0 nm.
- The present study utilizes Scanning Electron Microscopy (SEM). The surface morphology of the samples was examined using a Philips XL-30 SEM after they were gold-coated.

Fourier-transform infrared spectroscopy (FT-IR) is a analytical technique used to obtain information about the molecular composition of a substance by measuring the infrared spectrum. Spectra were obtained using a Shimadzu-8400s spectrometer in the range of 400–4000 cm-1. For the Fourier-transform infrared (FT-IR) analysis, each powder sample (1 mg) was meticulously mixed with 200 mg of IR-grade KBr (vacuum-dried) and subsequently compressed under a load of 8 tons to form transparent pellets.

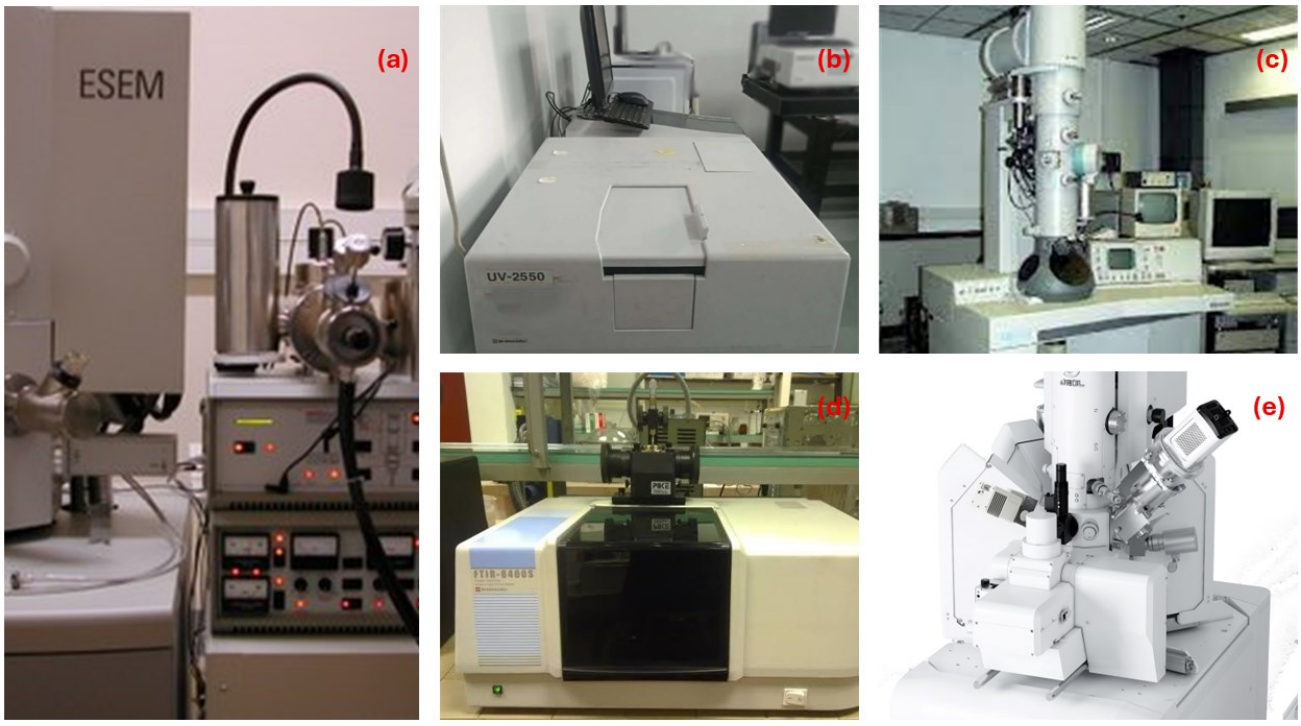

Figure 1. Techniques Used in this Study: (a) Scanning Electron Microscopy (SEM), (b) UV–Visible Spectroscopy (UV–Vis), (c) Transmission Electron Microscopy (TEM), (d) Fourier-Transform Infrared Spectroscopy (FT-IR), (e) X-ray Diffraction (XRD)

Results and Discussion

Hydrothermal Synthesis and Phase Stability of ZnS Nanostructures

ZnS nanostructures were successfully synthesized through the hydrothermal reaction between thiosemicarbazide, zinc nitrate hexahydrate, and a mixed solvent of ethylenediamine and water in a volume ratio of 3:2. The hydrothermal conditions, particularly the temperature and cooling rate, exerted a substantial influence on the purity and structural stability of the obtained ZnS phase. It was observed that maintaining the synthesis temperature at 200°C favored the formation of crystalline ZnS. However, under such conditions, a competing tendency for the formation of

the complex ZnS·0.5en is observed, where "en" denotes ethylenediamine.

In order to suppress this undesired side phase, the autoclave was subjected to rapid quenching in an ice bath immediately following the reaction. It is imperative to implement sudden cooling due to the reversible nature of the equilibrium between ZnS·0.5en and ZnS. A gradual cooling process increases the probability of the backward reaction, thereby stabilizing the complex phase rather than pure ZnS. As previously reported by Jiang et al. (2008), the reversible decomposition of ZnS·0.5en can be expressed as follows:

$$ZnS.0.5EN \leftrightarrow ZnS + 0.5EN \quad (1)$$

Consequently, rigorous regulation of the solvent ratio and the post-reaction cooling method emerged as pivotal for the successful synthesis of phase-pure ZnS nanostructures. The employment of ethylenediamine as a co-solvent not only augmented the solubility of the precursors but also functioned as a stabilizing ligand that could coordinate with Zn^{2+} ions, thereby exerting an influence on the nucleation and growth process. However, its incorporation into the crystal lattice is partial, resulting in the formation of the ZnS·0.5en complex. This observation underscores the delicate balance between its role as a stabilizer and its potential interference in phase formation.

The findings suggest that the selected hydrothermal parameters, particularly the solvent ratio and sudden quenching, are effective strategies to direct the reaction pathway toward the desired ZnS phase while preventing the growth of the ethylenediamine-containing byproduct. These findings underscore the significance of kinetic control during the hydrothermal process, which exerts a direct influence on the crystallinity, morphology, and purity of the resulting nanostructures.

FT-IR Spectral Analysis and Confirmation of ZnS Nanostructure Formation

The structural evolution of the synthesized ZnS nanostructures was further confirmed using Fourier Transform Infrared (FT-IR) spectroscopy. **Figure 2** presents the spectra of the ZnS sample prepared in KBr pellets, recorded before heating and after treatment under vacuum, respectively.

As illustrated in **Figure 2a**, the initial spectrum exhibited two prominent absorption peaks at 1629 cm^{-1} and 3444 cm^{-1}. These bands are attributed to the bending and stretching vibrations of the N–H group, respectively, which originate from residual ethylenediamine molecules coordinated with zinc ions during the synthesis process. The presence of these characteristic peaks indicates that the as-prepared product still contained organic residues or intermediate complexes, such as ZnS·0.5en.

To eliminate these residual organic groups, the compound was subjected to a controlled heat treatment under vacuum at 200 °C. The spectrum obtained after this treatment (**Figure 2b**) reveals the complete disappearance of the N–H related peaks, confirming the effective removal of ethylenediamine moieties and other volatile organic byproducts. The absence of significant intensity in this spectral region strongly indicates that the reaction proceeded to completion, yielding phase-pure ZnS nanostructures.

This spectral transformation provides clear evidence of the successful hydrothermal synthesis of ZnS and the critical role of post-synthesis vacuum heating in ensuring purity. The removal of organic groups not only validates the progress of the reaction but also enhances the crystallinity and stability of the nanostructures. Moreover, the absence of additional absorption bands in the fingerprint region corroborates the non-existence of other impurities, thereby validating that the observed IR profile corresponds to the anticipated ZnS phase.

A comprehensive examination of the FT-IR analysis reveals that a multifaceted approach encompassing hydrothermal synthesis and post-synthesis vacuum treatment is indispensable for the synthesis of high-purity ZnS nanostructures. This step is essential for the elimination of organic residues, which could otherwise interfere with the material's optical and electronic properties, thereby improving its suitability for advanced functional applications.

X-Ray Diffraction Analysis and Phase Identification of ZnS Nanostructures

The crystalline structure of the synthesized ZnS nanostructures was investigated using X-ray diffraction (XRD). The diffraction pattern is presented in **Figure 3**, and the obtained data were compared with the standard Joint Committee on Powder Diffraction Standards (JCPDS) card (No. 1314-98-3). The analysis confirmed that the product crystallized in the hexagonal wurtzite structure, with lattice constants determined as a = 3.820 Å and c = 6.257 Å.

The diffraction peaks observed in the experimental pattern correspond closely to those of the reference card, thereby confirming the formation of phase-pure ZnS without the presence of secondary phases such as zinc oxide or sulfur-related impurities. The sharpness and relative intensity of the peaks also suggest good crystallinity of the synthesized nanostructures.

A detailed comparison of the experimental diffraction peaks with the ASTM reference data is provided in **Table 1**. As demonstrated in Figure 1, the measured interplanar spacings (d values) and diffraction

angles (2θ) exhibit a high degree of congruence with the reported values in the JCPDS database. Characteristic reflections such as (100), (002), (101), (110), (103), and (112) planes were identified, thereby confirming the presence of the wurtzite phase. The slight variation observed between the standard and experimental d-spacing values may be attributed to nanoscale effects such as lattice strain, crystallite size reduction, or surface relaxation phenomena, which are commonly encountered in nanostructured materials.

The obtained diffraction pattern exhibited a high degree of consistency with the reference card, thereby providing robust validation of the successful synthesis of ZnS nanostructures with the desired wurtzite structure. These findings are consistent with the FT-IR results, which indicated the complete removal of residual organic species. Collectively, these results demonstrate that the hydrothermal process followed by vacuum treatment yields phase-pure crystalline ZnS.

In summary, the XRD analysis demonstrates that the employed hydrothermal synthesis route is effective in producing ZnS nanostructures with high structural purity and crystallinity. This structural integrity is of significant importance, as it directly influences the optical, electronic, and catalytic properties of ZnS, thereby enhancing its potential for applications in optoelectronics, photocatalysis, and sensing technologies.

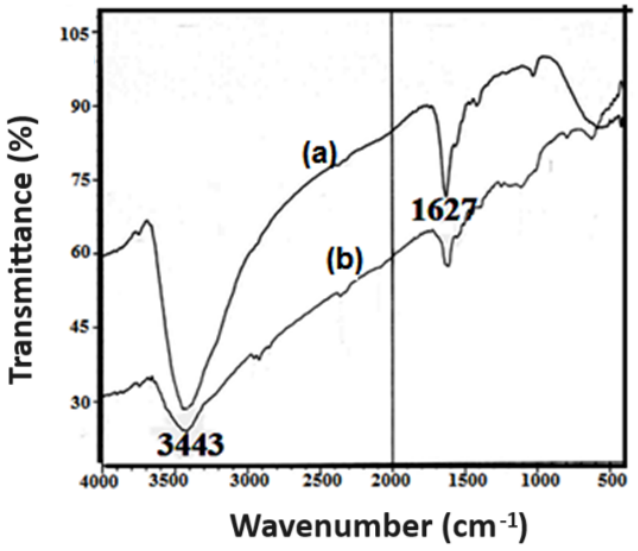

Figure 2. FT-IR Spectra of the Sample to form KBr Pellets, (a) Befor Heating, (b) After Heating.

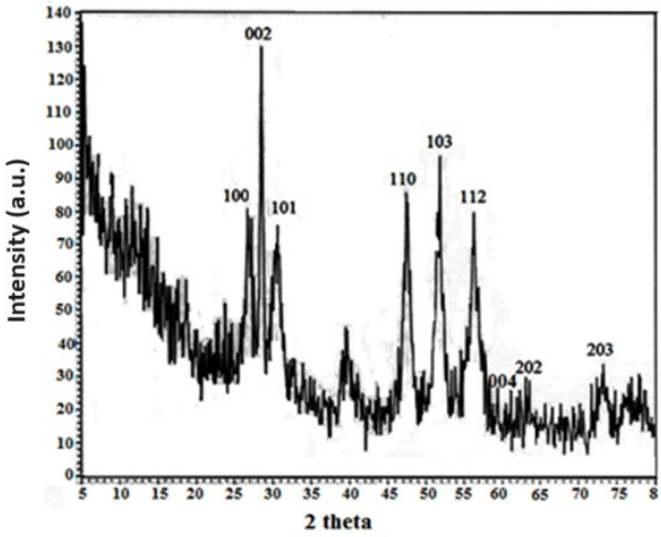

Figure 3. XRD Pattern of ZnS Nanostructure

Table 1. Comparing XRD Pattern of the Synthesized Sample with ASTM Card (JCPDS = 1314-98-3)

	Card ASTM (1314-98-3)	Sample
d(Å) (100) (2θ=26.80°)	3.30	3.32
d(Å) (0.02) (2θ=28.60°)	3.12	3.12
d(Å) (101) (2θ=30.60°)	2.92	2.92
d(Å) (110) (2θ=47.50°)	1.91	1.91
d(Å) (103) (2θ=51.90°)	1.76	1.76
d(Å) (112) (2θ=56.40°)	1.63	1.63
d(Å) (004) (2θ=59.50°)	1.56	1.56
d(Å) (202) (2θ=62.40°)	1.46	1.46
d(Å) (203) (2θ=73.30°)	1.29	1.29

Morphological Characterization of ZnS Nanostructures by SEM and TEM

The surface morphology and microstructural features of the synthesized ZnS nanostructures were examined using Scanning Electron Microscopy (SEM) and Transmission Electron Microscopy (TEM), as illustrated in **Figure 4a and b**. The SEM images revealed that the material exhibits a distinctive hedgehog-shaped morphology, consisting of spherical microscale structures densely covered with radially oriented nanorods. This hierarchical arrangement gives rise to a spiny surface texture, which is a characteristic feature of ZnS materials grown under controlled hydrothermal conditions.

A thorough examination through the use of a transmission electron microscope (TEM) revealed the nanoscale dimensions of these rod-like structures. The nanorods exhibited an average diameter of

approximately 5 nm, with uniform distribution and anchoring onto microspheres with diameters ranging between 1–2 μm. The observed hierarchical microsphere–nanorod architectures are consistent with previously reported ZnS morphologies (Gajendiran et al., 2020; Jubeer et al., 2023; Lim et al., 2022; Ru et al., 2021; Su et al., 2018; Wang et al., 2013; Xu et al., 2024; Zou et al., 2019).

The formation of hedgehog-like microstructures can be attributed to the oriented growth of ZnS nanorods, which nucleate on the microspherical cores and extend outward. This growth behavior is strongly influenced by the presence of ethylenediamine in the solvent system, which serves as a directing agent for the anisotropic growth of ZnS crystals. The resulting architecture increases the overall surface area of the material and provides unique textural features that may enhance its performance in catalytic, sensing, and optoelectronic applications.

Additionally, the uniform distribution of nanorods on the microspherical surfaces indicates a controlled nucleation and growth process during hydrothermal synthesis, underscoring the reproducibility and reliability of the adopted method. The hierarchical morphology is characterized by a dual-scale structure, incorporating microscale spheres that provide mechanical stability and nanoscale rods that facilitate functional activity. This integration of scales enables the convergence of the advantages inherent in both dimensions.

In summary, the results of the SEM and TEM analyses demonstrate that the hydrothermal process effectively yields ZnS nanostructures with a well-defined hedgehog-like morphology. This structural architecture not only verifies the growth mechanism but also opens pathways for enhancing the functional properties of ZnS in applications requiring high surface-to-volume ratios and efficient charge-transfer characteristics.

Optical Properties and Band Gap Energy Determination of ZnS Nanostructures

The optical behavior of the synthesized ZnS nanostructures was investigated using UV–Vis spectroscopy, and the corresponding spectra along with the Tauc plot analysis are presented in **Figure 5a and b**. The absorption spectrum was recorded in the wavelength range of 190–800 nm, where a strong absorption edge was observed at approximately 290 nm. This phenomenon is attributed to the electronic transition of electrons from the valence band to the conduction band, a characteristic of ZnS as a direct band gap semiconductor.

The optical band gap (Eg) of the ZnS nanostructures was calculated by analyzing the UV–Vis data using the Tauc relation (Arias Cerón et al., 2012), expressed as:

$$(\alpha h\nu)^n = B\,(h\nu - E_g) \qquad (2)$$

Where: α, the absorption coefficient; hν, the photon energy; Eg, the band gap energy; B, a proportionality constant; and n, the value assigned to indirect transitions (n = ½) and direct transitions (n = 2). The direct and indirect band gap energies were determined through a rigorous process of data analysis and graphical representation. Specifically, the (αhν)n versus hν plot was meticulously examined, and the linear portion of the curve was extrapolated to the energy axis. This methodical approach enabled the accurate determination of the band gap energies.

The calculated results indicated a direct band gap value that exceeded the typical range of bulk ZnS, which generally falls within the range of 3.6–3.7 eV. This observed increase, evidenced by the blue shift in the absorption edge compared to bulk ZnS (Zhou et al., 2016), is a clear indication of quantum confinement effects arising from the nanoscale dimensions of the synthesized structures. The reduction in particle size leads to spatial confinement of charge carriers, thereby widening the band gap and shifting the absorption to shorter wavelengths.

The blue-shifted absorption feature and enlarged band gap are significant because they directly enhance the optical and electronic properties of ZnS nanostructures. Materials with widened band gaps have been shown to possess significant promise for applications in optoelectronic devices, ultraviolet light-emitting diodes (UV-LEDs), photocatalysis, and sensing technologies, where the capacity for enhanced electron–hole separation and high-energy photon absorption is paramount.

In summary, the UV–Vis spectral analysis confirms that the ZnS nanostructures synthesized via hydrothermal processing exhibit pronounced quantum confinement effects, as demonstrated by their shifted absorption edge and widened band gap energy. These results underscore the efficacy of the adopted synthesis strategy in tailoring the optical properties of ZnS at the nanoscale for advanced functional applications.

Photocatalytic Properties of ZnS Nanostructure

The photocatalytic activity of the synthesized ZnS nanostructures was evaluated using methyl orange (MO) dye as a model organic pollutant. The stock solution was prepared by initially dissolving 0.00375 g of methyl orange in 1000 mL of distilled water. From this solution, 100 milliliters were withdrawn, and the pH was adjusted to 2 or 5 using 1 M HCl to study the effect of acidity on the degradation process. Subsequently, 0.075 g of ZnS photocatalyst was added

to the prepared dye solution. Prior to the irradiation process, the suspension underwent a 30-minute magnetically stirred period in a dark environment, thereby facilitating the establishment of adsorption–desorption equilibrium between the dye molecules and the catalyst surface.

The solution was subsequently exposed to ultraviolet irradiation (160 W) for a duration ranging from one to five hours. As illustrated in **Figure 6a**, the UV-Vis spectra of the dye solution are presented at varying irradiation intervals, while **Figure 6b** demonstrates the corresponding kinetic degradation curve. The findings reveal a progressive decline in the maximum absorption peak of methyl orange with an increase in irradiation time, thereby confirming the continuous degradation of the dye. Following a five-hour exposure period, approximately 75% degradation of methyl orange was achieved, indicating the strong photocatalytic performance of the ZnS nanostructures.

The efficiency of dye degradation is influenced by several parameters, including the dosage of the catalyst, the pH of the solution, the duration of the irradiation, and the intensity of the light source. Under UV irradiation, methyl orange molecules initially absorb energy and are excited to the singlet state (MO^1). The transition of these excited molecules to the triplet state (MO^3) is facilitated by intersystem crossing (ISC). At this stage, the photocatalyst has the capacity to accept an electron from the triplet dye molecules, resulting in the dye being placed in a positively charged state (MO^+). The conduction band of ZnS is subsequently replenished with electrons by dissolved oxygen in the solution, which acts as an electron scavenger.

The dye cations (MO^+) react rapidly with hydroxide ions (OH^-) in solution to generate hydroxyl radicals (•OH), while additional reactive oxygen species, such as superoxide radicals ($O_2•^-$), are also formed. These radicals possess high reactivity, which enables them to break the molecular bonds of the dye, including N=N, C–C, C=N, C–N, and C–S bonds. These bonds are adsorbed on the surface of the photocatalyst. This process leads to the mineralization of methyl orange into smaller, non-toxic inorganic species such as CO_2, SO_4^{2-}, Cl-, NO^{3-}, and NH^+ (Meena & Meena, 2010).

The photocatalytic mechanism can thus be summarized as a synergistic effect of light-induced electron–hole pair generation, reactive radical formation, and oxidative decomposition of the dye molecules. As the duration of the irradiation is increased, the concentration of •OH and $O_2•^-$ radicals concomitantly rises, thereby accelerating the degradation rate. These findings are consistent with earlier reports in the literature, which emphasize the crucial role of solution pH, light intensity, and photocatalyst loading on the kinetics of dye degradation (Meena & Kumar, 2011).

The overall degradation mechanism can be described through the following key steps, represented by equations (3 - 8):

$$\text{Methyl Orange} \xrightarrow[\text{ISC}]{\text{Light Radiations}} \text{Methyl Orange}^{*1} \quad (3)$$

$$\text{Methyl Orange}^{*1} \longrightarrow \text{Methyl Orange}^{*3} \quad (4)$$

$$\text{Methyl Orange}^{*3} + \text{I-R} \longrightarrow \text{Methyl Orange}^{+} + \text{I-R}\,(e^{-}) \quad (5)$$

$$\text{I-R}\,(e^{-}) + O_2 \longrightarrow \text{I-R} + {}^{-}O_2 \quad (6)$$

$$\text{Methyl Orange}^{+} + {}^{-}OH \longrightarrow \text{Methyl Orange} + {}^{-}OH^{\bullet} \quad (7)$$

$$\text{Methyl Orange} + OH^{\bullet} \longrightarrow \text{Product} \quad (8)$$

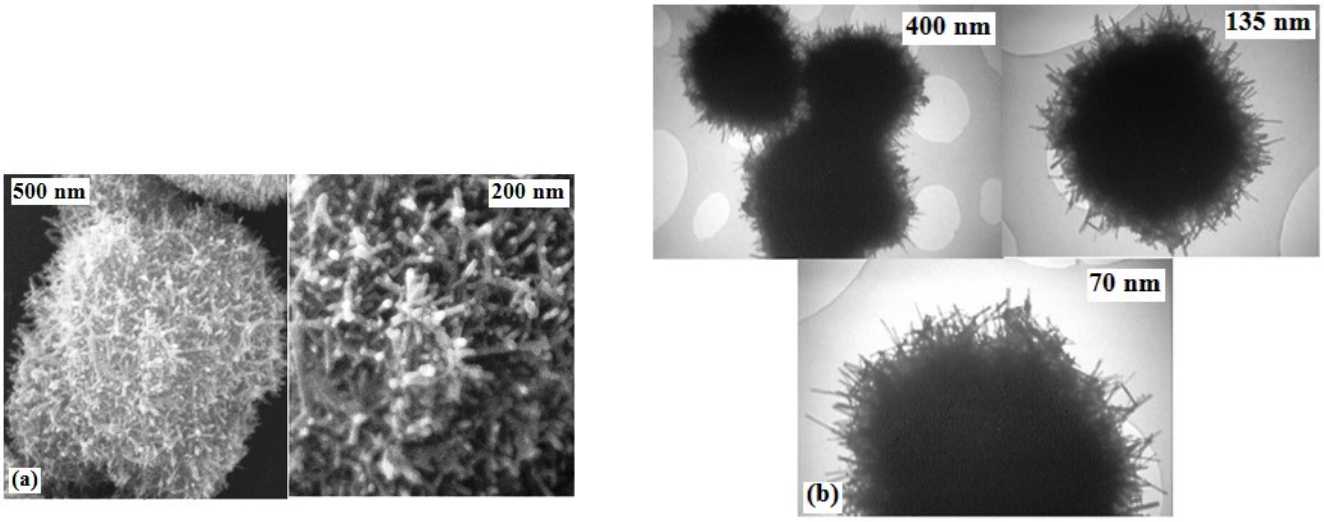

Figure 4. Images of Hedgehog -Shaped Nanostructure, (a) SEM, (b) TEM

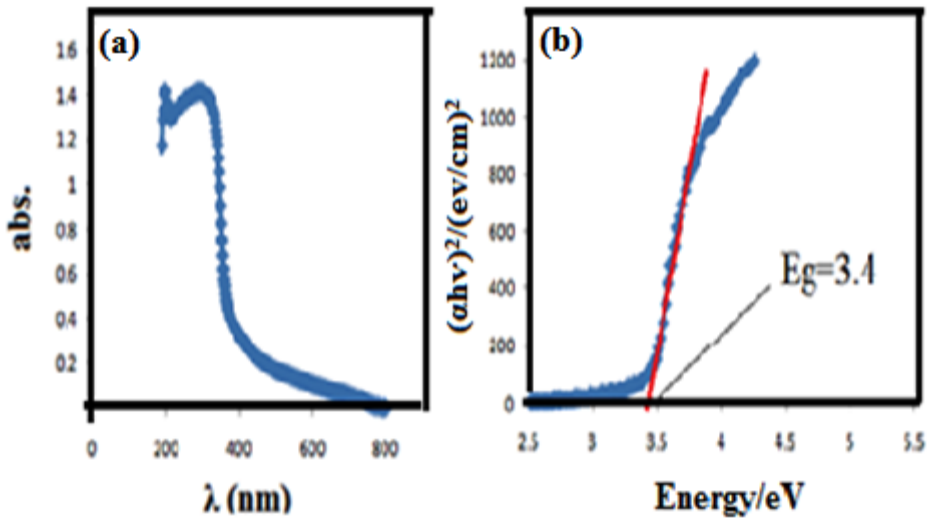

Figure 5. UV-Vis Graph of ZnS Nanostructure, (a) Electron Spectra, (b) Graph for the Band Gap Energy

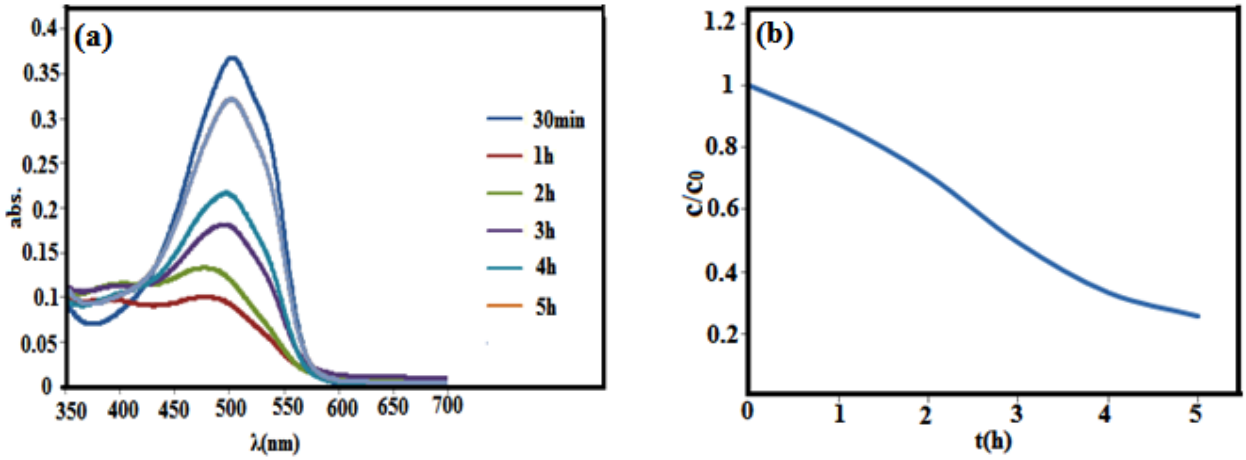

Figure 6. UV-Vis Graph, (a) for the Degradiation of Methyl Orange Dye by the Obtained Sample, (b) Kinetic Graph

Environmental Engineering Applications

The elimination of hazardous dyes and organic pollutants from industrial wastewater continues to be a pivotal challenge in the domain of environmental engineering. Effluents from the textile, printing, and pharmaceutical industries frequently contain synthetic dyes, such as methyl orange, which are toxic, non-biodegradable, and capable of generating carcinogenic byproducts in aquatic environments. Conventional treatment methods, including coagulation, adsorption, and biological degradation, frequently prove inadequate due to incomplete removal or the occurrence of secondary pollution. Photocatalysis, as an advanced oxidation process (AOP), offers an attractive alternative because it relies on semiconductor materials to generate highly reactive species (e.g., hydroxyl radicals) that can fully mineralize organic contaminants into CO_2, H_2O, and inorganic ions (Isac & Enesca, 2022; Lee & Wu, 2017).

ZnS-based nanostructures, particularly those with hierarchical morphologies, have been identified as promising photocatalysts for wastewater treatment applications. The hedgehog-shaped ZnS nanostructures synthesized in this study offer distinct advantages due to their radially oriented nanorods and microsphere assemblies. This geometry has been demonstrated to enhance light absorption, increase the number of exposed active sites, and promote multidirectional scattering, thereby improving photocatalytic efficiency. As indicated in the works of Jubeer et al. (2023) and Kozhevnikova et al. (2022), analogous structural strategies have been documented in ZnS composites and doped systems. These systems have been observed to exhibit enhanced pollutant degradation performance under UV and visible light irradiation. The present study demonstrates the practical potential of ZnS nanostructures as an effective treatment material for industrial effluents, as evidenced by the 75% degradation of methyl orange dye.

Beyond the removal of dyes, ZnS nanostructures boast broader environmental engineering applications, including integration into solar-driven photocatalytic reactors, coating of reactive membranes for water purification, and hybridization with other semiconductors (e.g., TiO_2, ZnO, CdS) to expand

visible light absorption. Recent studies have emphasized the scalability of ZnS-based photocatalysts for real-world applications, noting their relatively low toxicity compared to cadmium sulfide and their alignment with sustainable material selection principles (Boulkroune et al., 2019; Ücker et al., 2023). Consequently, hedgehog-shaped ZnS nanostructures have the potential to serve as a foundation for developing next-generation green technologies in wastewater management and environmental remediation.

Conclusion

This study successfully demonstrated the hydrothermal synthesis of hedgehog-shaped ZnS nanostructures and comprehensively evaluated their structural, morphological, optical, and photocatalytic properties. The combination of characterization techniques—including FT-IR, XRD, SEM, TEM, and UV–Vis spectroscopy—confirmed the formation of phase-pure ZnS with a wurtzite structure, nanoscale crystallinity, and unique hierarchical architecture. The photocatalytic degradation of methyl orange dye under UV irradiation further validated the potential of ZnS nanostructures as efficient catalysts for environmental remediation.

The following conclusions can be drawn:

- The application of hydrothermal processing at 200°C, in conjunction with the precise modulation of solvent ratios and the expeditious quenching of the process, resulted in the isolation of phase-pure ZnS. This approach precluded the formation of undesired ZnS·0.5en complexes.

- XRD analysis confirmed the presence of the wurtzite crystalline phase, while SEM and TEM revealed hedgehog-like microspheres decorated with 5 nm nanorods. These nanorods provide the microspheres with a high surface area and structural stability.

- UV–Vis spectroscopy revealed a blue shift in the absorption edge when compared to bulk ZnS, a phenomenon attributed to quantum confinement effects. This results in an enlarged band gap energy, which in turn enhances optical activity.

- ZnS nanostructures demonstrated notable photocatalytic degradation capabilities, achieving approximately 75% removal of methyl orange dye within a 5-hour period under UV irradiation. The mechanism involved the generation of hydroxyl and superoxide radicals, which drove the oxidative breakdown of dye molecules into harmless end-products.

While this work establishes ZnS nanostructures as promising candidates for photocatalytic and optoelectronic applications, further studies are needed to broaden their practical utility. Future research endeavors should concentrate on enhancing visible-light responsiveness through doping, heterojunction engineering, or surface modification to broaden the range of applications beyond UV-driven catalysis. Furthermore, the implementation of long-term stability tests, the expansion of synthesis methods, and the integration of these nanostructures into real wastewater systems would serve to enhance the environmental relevance of the subject. Finally, the integration of ZnS with other semiconductors to form hybrid nanocomposites has the potential to enhance charge separation efficiency and photocatalytic performance, thereby opening pathways for both energy and environmental applications.

Declarations

Authors' Contributions

M.H: Conceptualization, Methodology, Validation, Resources, Writing of the original draft.

A.KH: Conceptualization, Methodology, Validation, Formal analysis, Resources, Writing of the original draft.

A.T: Conceptualization, Investigation, Writing – review & editing, Supervision.

Conflict of Interest

The authors declare that they have no known competing financial interests or personal relationships that could have appeared to influence the work reported in this paper.

Funding

This research did not receive any specific grant from funding agencies in the public, commercial, or not-for-profit sectors.

Declaration on the Use of Generative AI and AI-Assisted Technologies

We acknowledge that generative AI and AI-assisted technologies were employed in the refinement of this manuscript to enhance the clarity, coherence, and overall quality of the writing.

Data Availability

The data that support the findings of this study are available from the corresponding author upon reasonable request.

Acknowledgement

The authors are grateful to Iran University of Science and Technology for the providing materials and some facilities.

Ethics

This study did not involve human participants or animals; hence, no ethical approval was required.

References

Abd Al-Zahra, A., & Al-Sammarraie, A. K. M. A. (2021). Hydrothermal synthesis and characterization of zinc sulfide nanoparticles. *Eurasian Chemical Communications*, *3*(9), 606–613. https://doi.org/10.22034/ECC.2021.293399.1196

Arias Cerón, J. S., González Araoz, M. P., Bautista Hernández, A., Sánchez Ramírez, J. F., Herrera Pérez, J. L., & Mendoza Álvarez, J. G. (2012). Semiconductor Nanocrystals of InP@ZnS: Synthesis and Characterization. *Superficies y Vacío*, *25*(2), 134–138. https://superficiesyvacio.smctsm.org.mx/index.php/SyV/article/view/218

Boulkroune, R., Sebais, M., Messai, Y., Bourzami, R., Schmutz, M., Blanck, C., Halimi, O., & Boudine, B. (2019). Hydrothermal synthesis of strontium-doped ZnS nanoparticles: structural, electronic and photocatalytic investigations. *Bulletin of Materials Science*, *42*(5), 223. https://doi.org/10.1007/s12034-019-1905-2

Gajendiran, J., Gnanam, S., Vijaya Kumar, V., Ramachandran, K., Ramya, J. R., Gokul Raj, S., & Sivakumar, N. (2020). Structural, optical and photocatalytic properties of ZnS spherical/flake nanostructures by sugar-assisted hydrothermal process. *Chemical Physics Letters*, *754*, 137639. https://doi.org/10.1016/j.cplett.2020.137639

Houshmand, R., & Emrooz, H. B. M. (2019). Photocatalytic outcomes for methylene blue degradation from CTAB mediated mesoporous ZnS, synthesized with an insoluble precursor in ethanol media. *Nanochemistry Research*, *4*(1), 64–76. https://doi.org/10.22036/NCR.2019.01.008

Ibupoto, Z., Khun, K., Liu, X., & Willander, M. (2013). Hydrothermal Synthesis of Nanoclusters of ZnS Comprised on Nanowires. *Nanomaterials*, *3*(3), 564–571. https://doi.org/10.3390/nano3030564

Isac, L., & Enesca, A. (2022). Recent Developments in ZnS-Based Nanostructures Photocatalysts for Wastewater Treatment. *International Journal of Molecular Sciences*, *23*(24), 15668. https://doi.org/10.3390/ijms232415668

Jiang, C., Zhang, W., Zou, G., Yu, W., & Qian, Y. (2007). Hydrothermal synthesis and characterization of ZnS microspheres and hollow nanospheres. *Materials Chemistry and Physics*, *103*(1), 24–27. https://doi.org/10.1016/j.matchemphys.2006.11.001

Jiang, L., Yang, M., Zhu, S., Pang, G., & Feng, S. (2008). Phase Evolution and Morphology Control of ZnS in a Solvothermal System with a Single Precursor. *The Journal of Physical Chemistry C*, *112*(39), 15281–15284. https://doi.org/10.1021/jp804705v

Jubeer, E. M., Manthrammel, M. A., Subha, P. A., Shkir, M., Biju, K. P., & AlFaify, S. A. (2023). Defect engineering for enhanced optical and photocatalytic properties of ZnS nanoparticles synthesized by hydrothermal method. *Scientific Reports*, *13*(1), 16820. https://doi.org/10.1038/s41598-023-43735-1

Kozhevnikova, N. S., Melkozerova, M. A., Enyashin, A. N., Tyutyunnik, A. P., Pasechnik, L. A., Baklanova, I. V., Suntsov, A. Yu., Yushkov, A. A., Buldakova, L. Yu., & Yanchenko, M. Yu. (2022). Janus ZnS nanoparticles: Synthesis and photocatalytic properties. *Journal of Physics and Chemistry of Solids*, *161*, 110459. https://doi.org/10.1016/j.jpcs.2021.110459

Lee, G.-J., & Wu, J. J. (2017). Recent developments in ZnS photocatalysts from synthesis to photocatalytic applications — A review. *Powder Technology*, *318*, 8–22. https://doi.org/10.1016/j.powtec.2017.05.022

Liang, X., Xing, L., Xiang, J., Zhang, F., Jiao, J., Cui, L., Song, B., Chen, S., Zhao, C., & Sai, H. (2012). The Role of the Liquid–Liquid Interface in the Synthesis of Nonequilibrium Crystalline Wurtzite ZnS at Room Temperature. *Crystal Growth & Design*, *12*(3), 1173–1179. https://doi.org/10.1021/cg2011474

Lim, T., Seol, S. K., Kim, H.-J., Huh, Y. H., Jung, Y., Chung, H.-S., & Kim, J. H. (2022). In situ synthesis of hierarchically-assembled three-dimensional ZnS nanostructures and 3D printed visualization. *Scientific Reports*, *12*(1), 16955. https://doi.org/10.1038/s41598-022-21297-y

Meena, R. C., & Kumar, V. (2011). Studies on photodegradation of Tropaeolin O (Acid Orange 6) in aqueous solution using immobilized Dowex-11 photocatalyst. *Journal of the Indian Chemical Society*, *88*, 257–264.

Motejadded Emrooz, H. B., & Rahmani, A. R. (2017). Synthesis, characterization and photocatalytic behavior of mesoporous ZnS nanoparticles prepared by hybrid salt extraction and structure directing agent method. *Materials Science in Semiconductor Processing*, *72*, 15–21. https://doi.org/10.1016/j.mssp.2017.08.018

Riazian, M. (2023). Enhancement of the photocatalytic activity of fabricated ZnS nanoparticles in the photodegradation of methylene blue. *Physica Scripta*, *98*(6), 065956. https://doi.org/10.1088/1402-4896/acd036

Riazian, M., & Yekrangisendi, A. (2023). Synthesis of ZnS Nanoparticles via a Sonochemical

Method: Photocatalytic Activity and Optical Properties. *Physical Chemistry Research*, *11*(3), 575–587. https://doi.org/10.22036/PCR.2022.341626.2099

Ru, F., Xia, J., Li, X., Wang, Y., Hua, Z., Shao, R., Wang, X., Lee, C.-S., & Meng, X.-M. (2021). Al 2 O 3 buffer-facilitated epitaxial growth of high-quality ZnO/ZnS core/shell nanorod arrays. *Nanoscale*, *13*(26), 11525–11533. https://doi.org/10.1039/D1NR02613E

Sabaghi, V., Davar, F., & Fereshteh, Z. (2018). ZnS nanoparticles prepared via simple reflux and hydrothermal method: Optical and photocatalytic properties. *Ceramics International*, *44*(7), 7545–7556. https://doi.org/10.1016/j.ceramint.2018.01.159

Su, Q., Zou, R., Su, Y., & Fan, S. (2018). Morphology Control and Growth Mechanism Study of Quantum-Sized ZnS Nanocrystals from Single-Source Precursors. *Journal of Nanoscience and Nanotechnology*, *18*(10), 6850–6858. https://doi.org/10.1166/jnn.2018.15516

Ücker, C. L., Almeida, S. R., Cantoneiro, R. G., Diehl, L. O., Cava, S., Moreira, M. L., Longo, E., & Raubach, C. W. (2023). Study of CaTiO3–ZnS heterostructure obtained by microwave-assisted solvothermal synthesis and its application in photocatalysis. *Journal of Physics and Chemistry of Solids*, *172*, 111050. https://doi.org/10.1016/j.jpcs.2022.111050

Viswanath, R., Naik, H. S. B., Somalanaik, Y. K. G., Neelanjeneallu, P. K. P., Harish, K. N., & Prabhakara, M. C. (2014). Studies on Characterization, Optical Absorption, and Photoluminescence of Yttrium Doped ZnS Nanoparticles. *Journal of Nanotechnology*, *2014*, 1–8. https://doi.org/10.1155/2014/924797

Wang, G., Huang, B., Li, Z., Lou, Z., Wang, Z., Dai, Y., & Whangbo, M.-H. (2015). Synthesis and characterization of ZnS with controlled amount of S vacancies for photocatalytic H2 production under visible light. *Scientific Reports*, *5*(1), 8544. https://doi.org/10.1038/srep08544

Wang, H., Chen, Z., Cheng, Q., & Yuan, L. (2009). Solvothermal synthesis and optical properties of single-crystal ZnS nanorods. *Journal of Alloys and Compounds*, *478*(1–2), 872–875. https://doi.org/10.1016/j.jallcom.2008.12.039

Wang, J., You, T., Feng, H., Chen, K., & Xu, B. (2013). Selective synthesis of ZnS nanowire-bundles and nanowires via different growth mechanisms. *Journal of Crystal Growth*, *374*, 60–64. https://doi.org/10.1016/j.jcrysgro.2013.03.050

Xu, S. H., Fei, G. T., Huang, J. Y., Xia, K., & Wang, B. (2024). Controllable hydrothermal synthesis of hollow ZnS nanospheres: Morphological evolution mechanism and photocatalytic performance. *Ceramics International*, *50*(1), 1556–1563. https://doi.org/10.1016/j.ceramint.2023.10.247

Zhou, D.-J., Xie, X.-Y., Zhang, Y., Guo, D.-Y., Zhou, Y.-J., & Xie, J.-F. (2016). Facile synthesis of ZnS nanorods in PEG and their spectral performance. *Materials Research Express*, *3*(10), 105023. https://doi.org/10.1088/2053-1591/3/10/105023

Zou, Z., Yang, X., Zhang, P., Zhang, Y., Yan, X., Zhou, R., Liu, D., Xu, L., & Gui, J. (2019). Trace carbon-hybridized ZnS/ZnO hollow nanospheres with multi-enhanced visible-light photocatalytic performance. *Journal of Alloys and Compounds*, *775*, 481–489. https://doi.org/10.1016/j.jallcom.2018.10.116